

A CUBESAT FOR CALIBRATING GROUND-BASED AND SUB-ORBITAL MILLIMETER-WAVE POLARIMETERS (CALSAT)

BRADLEY R. JOHNSON¹, CLEMENT J. VOURCH², TIMOTHY D. DRYSDALE², ANDREW KALMAN³,
STEVE FUJIKAWA⁴, BRIAN KEATING⁵ AND JON KAUFMAN⁵

¹*Department of Physics, Columbia University, New York, NY 10027, USA*

²*School of Engineering, University of Glasgow, Glasgow, Scotland G12 8QQ, UK*

³*Pumpkin, Inc., San Francisco, CA 94112, USA*

⁴*Maryland Aerospace Inc., Crofton, MD 21114, USA*

⁵*Department of Physics, University of California, San Diego, CA 92093-0424, USA*

Received (to be inserted by publisher); Revised (to be inserted by publisher); Accepted (to be inserted by publisher);

We describe a low-cost, open-access, CubeSat-based calibration instrument that is designed to support ground-based and sub-orbital experiments searching for various polarization signals in the cosmic microwave background (CMB). All modern CMB polarization experiments require a robust calibration program that will allow the effects of instrument-induced signals to be mitigated during data analysis. A bright, compact, and linearly polarized astrophysical source with polarization properties known to adequate precision does not exist. Therefore, we designed a space-based millimeter-wave calibration instrument, called CalSat, to serve as an open-access calibrator, and this paper describes the results of our design study. The calibration source on board CalSat is composed of five “tones” with one each at 47.1, 80.0, 140, 249 and 309 GHz. The five tones we chose are well matched to (i) the observation windows in the atmospheric transmittance spectra, (ii) the spectral bands commonly used in polarimeters by the CMB community, and (iii) The Amateur Satellite Service bands in the Table of Frequency Allocations used by the Federal Communications Commission. CalSat will be placed in a polar orbit allowing visibility from observatories in the Northern Hemisphere, such as Mauna Kea in Hawaii and Summit Station in Greenland, and the Southern Hemisphere, such as the Atacama Desert in Chile and the South Pole. CalSat also will be observable by balloon-borne instruments launched from a range of locations around the world. This global visibility makes CalSat the only source that can be observed by all terrestrial and sub-orbital observatories, thereby providing a universal standard that permits comparison between experiments using appreciably different measurement approaches.

Keywords: CMB Polarization, CubeSat, Calibration, B-modes.

1. Introduction

In this paper, we describe a low-cost, open-access, CubeSat-based calibration instrument called CalSat that is designed to support ground-based and sub-orbital experiments searching for various polarization signals in the cosmic microwave background (CMB). The CMB is a bath of photons that permeates all of space and carries an image of the Universe as it was 380,000 years after the Big Bang. This image spans the entire sky, but it is not visible to the human eye because the frequency spectrum of the CMB peaks in the millimeter-wave region of the electromagnetic spectrum. Physical processes that operated in the universe when the CMB formed left an imprint that can be detected today. This imprint is observed as angular intensity and linear polarization anisotropies. These primordial CMB anisotropies have proven to be a treasure trove of cosmological information. For example, the precise characterization of the intensity (or temperature) anisotropy of the CMB has helped reveal that spacetime is flat, the universe is 13.8 billion

¹bjohnson@phys.columbia.edu

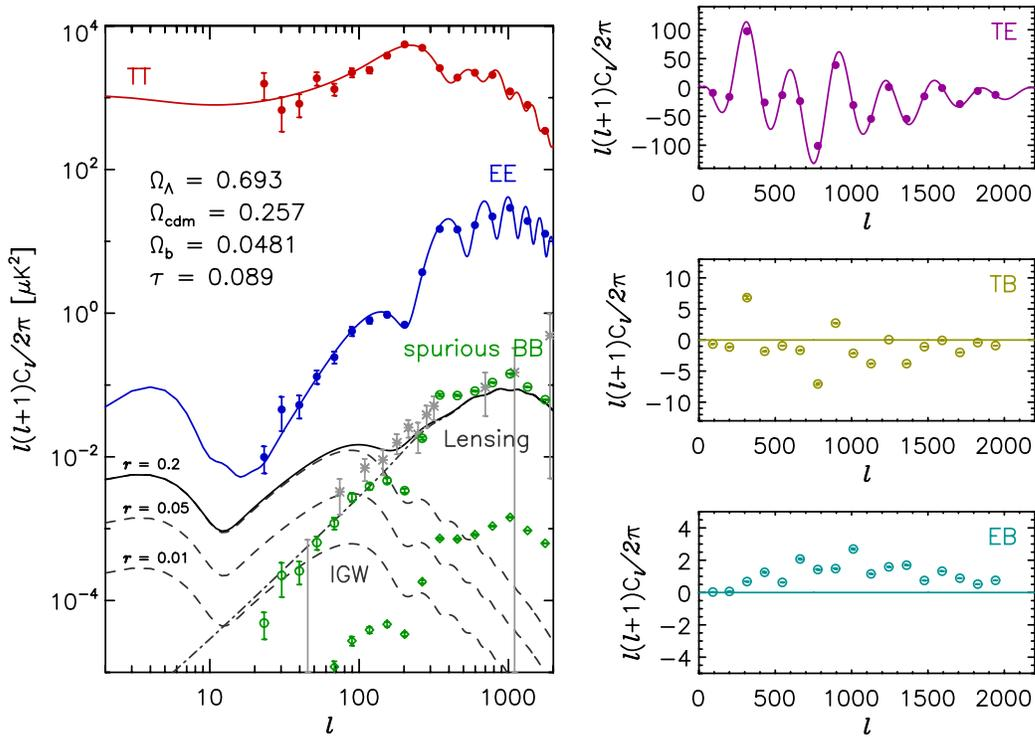


Fig. 1. Angular power spectra for various CMB signals. The solid curves are models computed using the current best-fit cosmological parameters. Data points from an experiment simulation (circles and diamonds) and measurements from the POLARBEAR Collaboration [2014] and the BICEP2/Keck and Planck Collaborations [2015] (grey stars) are plotted along with these curves for comparison. On the left, the red curve corresponds to the temperature signal, the blue curve corresponds to the E-mode signal, and the black curve is the expected B-mode signal, which includes both an inflationary gravitational wave (IGW) component (dashed) for $r = 0.2$ and a non-primordial B-mode signal that is produced when large-scale structure converts E-modes to B-modes via gravitational lensing (dash-dot). For comparison, IGW signal curves for $r = 0.01$ and 0.05 are also plotted. The TE, TB and EB power spectra are plotted on the right. The details of the experiment simulation, which shows the effect of instrument-induced polarization rotation, are discussed in Section 2. The green circles and diamonds show the spurious BB signal for 2.0 deg and 0.2 deg of polarization rotation, respectively.

years old, and the energy content of the universe is dominated by cold dark matter and dark energy [see for example, Bennett *et al.*, 2013; Planck Collaboration, 2014]. The density inhomogeneities that produced the detected temperature anisotropies theoretically should generate, through Thomson scattering during the epoch of recombination, a curl-free polarization signal known as “E-mode” polarization. This companion signal has also been observed at the theoretically expected level providing further confidence in the Λ CDM cosmological model [see for example, Naess *et al.*, 2014; Crites *et al.*, 2015; BICEP2 Collaboration, 2014a; QUIET Collaboration, 2011; Brown *et al.*, 2009].

The inflationary cosmological paradigm posits that a burst of exponential spacetime expansion, called inflation, took place during the first fraction of a second after the Big Bang. Observational evidence to date supports this paradigm and has given it a strong footing, though the precise physical mechanism that caused inflation is unknown. Inflation should have produced a stochastic background of gravitational waves. These gravitational waves would have produced polarization signals separable from E-modes by their divergence-free “B-mode” signature [Zaldarriaga & Seljak, 1997; Kamionkowski *et al.*, 1997]. The magnitude of this inflationary gravitational wave (IGW) B-mode signal is proportional to the energy scale at which inflation occurred. See for example, the dashed curves in Figure 1 and note that the IGW signal amplitude is commonly parameterized as r , the so-called tensor-to-scalar ratio, which is related to

the energy scale of inflation¹ [Baumann *et al.*, 2009; Knox & Song, 2002]. If the IGW signal ultimately is discovered, then the energy scale of inflation would be experimentally ascertained. This measurement would place a tight constraint on the theoretical models that describe the inflation mechanism, and this constraint would be a breakthrough for both astrophysics and particle physics because there is no way to create inflation-like conditions in a laboratory or particle accelerator. The IGW signal is currently the primary focus of CMB research, and we will discuss the status of current measurements at the end of Section 2.

In addition to the IGW signal, other CMB polarization signals promise to deliver valuable cosmological information. Non-primordial B-modes are generated when E-modes are gravitationally lensed by large-scale structures in the Universe (see the dash-dot curve in Figure 1). This lensing B-mode signal is sensitive to physical parameters such as the sum of the neutrino masses [Abazajian *et al.*, 2015a]. B-mode polarization can also be used to probe physics outside the standard cosmological picture. Temperature to B-mode correlations (TB) and E-mode and B-mode correlations (EB) are expected to vanish in the standard model. Therefore, these estimators are sensitive probes for physics outside the standard model if the correlation signals are found to be non-zero. A variety of candidate non-standard-model physical mechanisms that produce cosmological polarization rotation (CPR) already have been identified. Parity violation in the electromagnetic sector via a Chern-Simons coupling can produce TB and EB correlations [Kaufman *et al.*, 2014]. A coupling of a pseudo-scalar field to electromagnetism would violate the Einstein Equivalence Principle and would result in TB and EB correlations [Ni, 1977; Carroll *et al.*, 1991]. TB and EB correlations can also be used to test chiral gravity models [Gluscevic & Kamionkowski, 2010] and to search for primordial magnetic fields [Pogosian *et al.*, 2009; Yadav *et al.*, 2012].

2. Polarimeter Calibration

The magnitude of the forecasted TB, EB and B-mode signals is faint when compared with unavoidable instrument-induced systematic errors. Therefore, all experiments trying to measure these signals need a robust polarimeter calibration program that will allow the effect of these instrument-induced errors to be mitigated during data analysis. Several performance requirement studies have been published specifically for IGW searches [Bock *et al.*, 2006; O’Dea *et al.*, 2007; Bock *et al.*, 2009]. These studies indicate the level of systematic error that can be tolerated for a given IGW signal amplitude. For the CalSat design program we chose to use the performance requirements derived by the Task Force on Cosmic Microwave Background Research [Bock *et al.*, 2006] as a benchmark. This report proposes a general performance requirement where each systematic error must be suppressed to a factor of ten below an IGW signal corresponding to a tensor-to-scalar ratio of $r = 0.01$, which is the level where the gravitational lensing signal starts to dominate the IWG signal at $\ell = 100$.

Many of the known systematic errors can be mitigated straightforwardly. However, a *robust* mitigation strategy for instrument-induced polarization rotation (IPR), which is one of the most critical systematic errors, has not yet been identified. This instrumental effect rotates the apparent orientation of the linearly-polarized pseudo-vectors on the sky, and this rotation converts the brighter E-modes into spurious B-modes. Using the aforementioned performance requirement definition, any IPR must be limited to 0.2 deg for an IGW search targeting $r > 0.01$; fainter IGW signals would require a tighter constraint, and even more precision could be needed if delensing techniques ultimately will be used to probe below $r = 0.01$ [Smith *et al.*, 2012].

To illustrate this effect we performed a simple experiment simulation where a set of Stokes parameter maps (I , Q , U with $V = 0$) containing CMB signals were simulated and then the orientation of the polarization of each pixel was rotated by 2 deg using the Mueller matrix for linear polarization rotation. The input maps were 1000 deg², contained no noise or other beam effects, and all B-mode signals were set to zero. The angular power spectra of the corrupted maps were then estimated, and the estimated power spectra are shown in Figure 1. The open-circle points in this figure (BB, TB and EB) are spurious signals

¹The tensor-to-scalar ratio r is related to the energy scale of inflation as $V^{1/4} = 1.06 \times 10^{16} \left(\frac{r}{0.01}\right)^{1/4}$ [GeV].

	frequency [GHz]	I [Jy]	P [Jy]	P/I [%]	polarization angle uncertainty		total power [†] [fW]	polarized power [†] [fW]
					systematic [deg]	statistical [deg]		
Planck ^a	30	340	24	7.1	0.50	0.54	16	2.2
	44	290	19	6.5	0.50	0.32	20	2.5
	70	260	21	7.9	0.50	0.23	30	4.4
	100	220	16	7.2	0.62	0.11	35	4.8
	143	170	12	7.2	0.62	0.13	39	5.1
	217	120	10	8.1	0.62	0.12	42	6.5
	353	82	10	12	0.62	0.37	49	11
WMAP ^b	23	380	27	7.1	1.5	0.10	14	1.9
	33	340	24	6.9	1.5	0.10	18	2.4
	41	320	22	7.0	1.5	0.20	21	2.7
	61	280	19	7.0	1.5	0.40	27	3.5
	93	230	17	7.1	1.5	0.70	34	4.7
IRAM ^c	90	200	15	8.8	0.50	0.20	29	4.7
CalSat	47.1			100	0.05		2000	2000
	80.0			100	0.05		1300	1300
	140			100	0.05		130	130
	249			100	0.05		48	48
	309			100	0.05		23	23

^a Measurements from Planck Collaboration [2015] using the maximum likelihood filtering method

^b Measurements from Weiland *et al.* [2011]

^c Measurement from Aumont *et al.* [2010]

[†] Computed for this comparison assuming the detector is sensitive to a single polarization and the telescope aperture area is 1 m^2 for all cases. To convert the measurements from Planck, WMAP and IRAM from Jy to fW, we made the additional assumption that $\delta\nu/\nu_c = 0.3$

Table 1. A comparison between CalSat and Tau A measurements from Planck, WMAP and the IRAM telescope. The polarization angle uncertainty requirement from the Weiss Report is 0.2 deg [Bock *et al.*, 2006]. The available measurements of Tau A do not meet this specification because the smallest systematic error to date is 0.5 deg. Also, the high-resolution Aumont *et al.* [2010] measurement shows that the polarization intensity morphology of Tau A is complicated.

entirely produced by the polarization rotation operation. A rotation of just 2 deg creates a false B-mode signal that is comparable in magnitude to both the lensing signal and the sought-after IGW signal below $\ell \simeq 100$ if the tensor-to-scalar ratio is $r = 0.01$. The takeaway message is a very small amount of rotation can produce a false B-mode signal that can obscure the actual sky signal.

To properly characterize the IPR properties of a CMB polarimeter, a linearly polarized source with known polarization properties should be observed with high precision. This required calibration measurement provides the critical relationship between the coordinate system of the polarimeter in the instrument frame and the coordinate system on the sky that defines the astrophysical Q and U Stokes parameters. The ideal source should be point-like in the beam of the telescope and bright enough to generate high signal-to-noise calibration data with a reasonable amount of integration time. But this source should not be too bright, or it will saturate the detector system. Finally, the orientation of the polarization of the observed source on the sky must be known to 0.2 deg or better for $r > 0.01$. It is important to note that the magnitude of this systematic error typically varies across the focal plane of the telescope, so the IPR effect must be determined for each detector in any given instrument.

Many current experiments “self-calibrate” their polarization angles by assuming TB and EB correlations are zero [Keating *et al.*, 2013]. This self-calibration technique uses the TB and EB spectra on the right in Figure 1 along with the theoretical idea that these spectra should be zero in the absence of CPR to remove the green spurious B-mode points on the left. This approach makes it impossible to use B-mode, TB and EB measurements to constrain the aforementioned isotropic departures from the standard model (see Section 1) because any signal produced by CPR is incorrectly interpreted as an error signal. If this problem is avoided and self-calibration is not used, then the current achieved precision of ~ 0.5 deg severely limits the ability of experiments to search for any departures from standard cosmology via TB and EB measurements. A more precise calibration procedure is needed to make progress with CPR studies.

Some partially polarized astrophysical sources are available, and at millimeter-wavelengths, the best of these appears to be Tau A. Tau A is a supernova remnant located at Right ascension = 05 34 32 (hms) and Declination = +22 00 52 (dms), and it has an angular extent of $7' \times 5'$. For calibration, its most relevant properties are (i) the measured polarization angle uncertainty, (ii) the polarized fraction, and (iii) the source brightness. The WMAP satellite measured its polarization properties in spectral bands between 20 and 100 GHz [Weiland *et al.*, 2011], the Planck satellite measured its polarization properties in spectral bands between 30 and 353 GHz [Planck Collaboration, 2015], and Aumont *et al.* [2010] studied the suitability of Tau A as a calibration source for CMB studies at 90 GHz using the 30 m IRAM telescope. These measurements are summarized in Table 1. ACTpol [Naess *et al.*, 2014] and POLARBEAR [POLARBEAR Collaboration, 2014] recently observed Tau A as part of their respective calibration programs and showed that the polarization intensity morphology at 145 GHz is complicated.

Though Tau A is the best polarized source on the sky at millimeter wavelengths, it does not meet the performance requirements of a calibrator for an IGW-signal search. First and foremost, with a Declination = +22 00 52 (dms), it is not accessible to observatories at the South Pole or on Antarctic balloons. It can be observed from the Atacama Desert in Chile, though it will always be at a zenith angle of 45 deg or more. Second, it is not bright enough to give a high signal-to-noise ratio measurement with a short integration time. Third, the source is extended rather than point-like. And finally, the millimeter-wave spectrum of Tau A is not precisely known, though it is certainly not that of a 2.7 K blackbody. Polarimeters that have frequency-dependent performance, which is common, would need to precisely measure the frequency spectrum of Tau A before using it as a polarization angle calibrator (see Section 4).

Since an ideal *celestial* calibration source does not exist, some current experiments use ground-based sources for polarimeter calibration [BICEP2 Collaboration, 2014b; Crites *et al.*, 2015]. However, these measurements are challenging. For example, the Fraunhofer distance ($2D^2/\lambda$) for common telescopes is typically between 0.1 and 100 km, so the calibration source must be placed more than 0.1 to 100 km away, respectively, from the telescope for the desired far-field beam characterization measurement. This kind of measurement is difficult because the detector systems in CMB polarimeters are designed to observe sky backgrounds, which are typically ~ 10 K or less. To observe a ground-based calibration source more than 0.1 to 100 km away, the zenith angle of the telescope must be set to nearly 90 deg. Background loading from the large airmass and thermal emission from the ground at this zenith angle are high enough to saturate typical detector systems². Therefore two-stage bolometers or some kind of signal attenuator must be used for this style of calibration measurement. However, these approaches have their own varieties of systematic error, so awkwardly these calibration measurements could require their own calibration. A near-field measurement of a calibration source observed at smaller zenith angles can be performed instead to mitigate this high background loading problem. Yet, for the near-field measurement to be useful, a model-dependent theoretical correction must be applied to the data to derive the effective far-field calibration. This correction, however, also introduces uncertainty into the calibration, and the quality of the result depends entirely on the accuracy of this difficult theoretical calculation.

Current experiments are beginning to measure B-modes. The BICEP2 Collaboration recently announced a detection of degree-scale B-mode polarization in a 350 deg² patch of sky in the southern hemisphere [BICEP2 Collaboration, 2014a]. The POLARBEAR and SPTPol Collaborations detected B-mode polarization consistent with the aforementioned gravitational lensing signal on sub-degree scales [POLARBEAR Collaboration, 2014; Keisler *et al.*, 2015]. And the Planck Collaboration published a measurement of B-mode polarization from Galactic dust emission at 353 GHz [Adam *et al.*, 2014]. This combination of results has added energy to CMB studies because these measurements indicate that faint B-mode signals are there on the sky and that instruments are now sensitive enough to detect them. Currently, BICEP2 and POLARBEAR use the aforementioned self-calibration technique, so it is impossible to use these measurements to constrain isotropic departures from the standard model. These results have re-emphasized the need for enhanced foreground discrimination capabilities and robust systematic error control; the latter effect being the major motivation behind CalSat.

²Here we are assuming bolometric detectors are being used. Bolometers are commonly used in CMB observations.

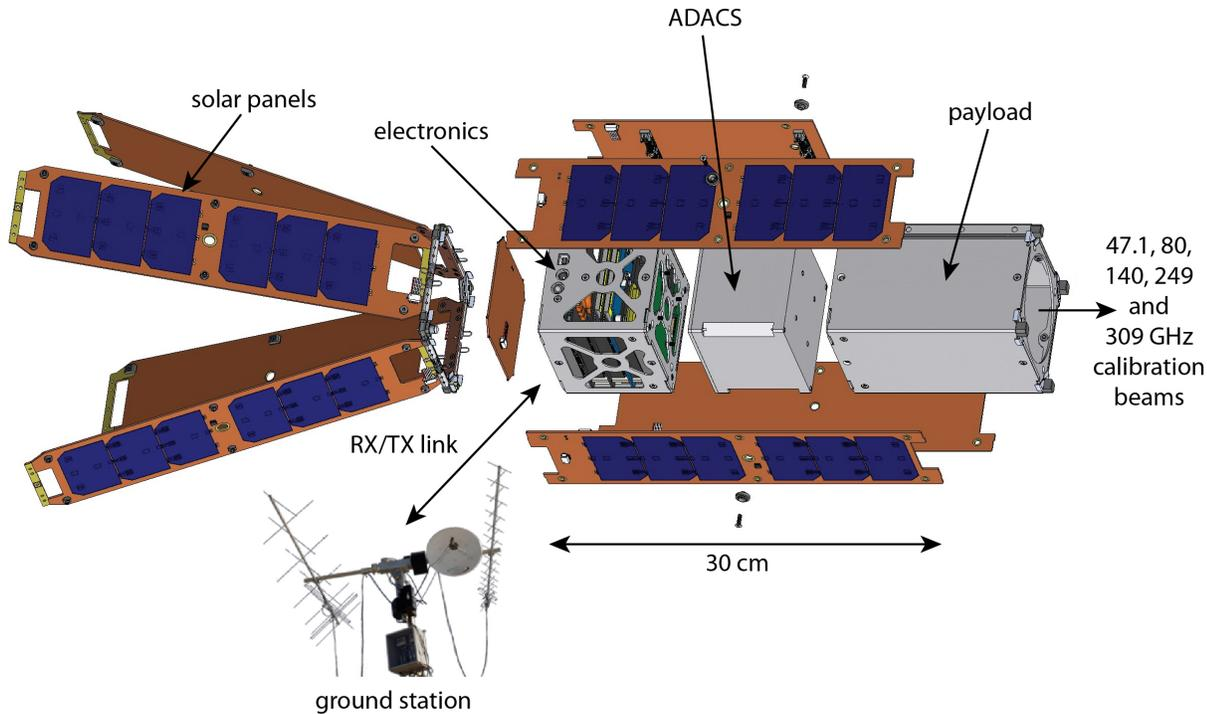


Fig. 2. An exploded view of CalSat. The four CalSat subsystems can all be seen. The payload section contains the millimeter-wave calibration sources (see Figures 3 & 4). The attitude determination and control system (ADACS) measures the CubeSat attitude and rotates the spacecraft as needed (see Figure 3). The electronics subsystem contains the on-board computer and the power system. The solar panels are electrically connected to this subsystem. Note that the power budget was computed using double-sided deployable solar panels, which are not shown for clarity. The ground station is used to upload commands and download attitude and housekeeping data. The technical details of the hardware components shown in this figure are given in Section 3.2.

3. Technical Approach

3.1. What are CubeSats?

A CubeSat-based instrument like the one we designed is composed of a “bus,” a payload and a ground station. These components can be seen in Figure 2. The bus includes the mechanical frame, the power system, solar panels, the on-board computer and electronics, an attitude determination and control system (ADACS), and a transmitter/receiver. The payload is the scientific experiment, which is mounted inside the bus. For CalSat the payload is the calibration instrument. The ground station includes a transmitter/receiver and computers, and it is used to download data and upload commands. It serves as the point of contact between the research team and the orbiting spacecraft.

CubeSats essentially get a free ride into orbit as auxiliary payloads. A Poly Picosatellite Orbital Deployer (P-POD) is installed in a rocket alongside its primary payload. CubeSats are loaded into the P-POD, and the P-POD jettisons the CubeSats at the appropriate time after launch. The P-POD defines the CubeSat standard, and CubeSats must conform to a strict list of requirements³ so that they are compatible with the P-POD. Among these requirements is a volume requirement. The fundamental CubeSat size is $10\text{ cm} \times 10\text{ cm} \times 10\text{ cm}$, and this size is referred to as “1U,” but larger 2U ($10\text{ cm} \times 10\text{ cm} \times 20\text{ cm}$) and 3U ($10\text{ cm} \times 10\text{ cm} \times 30\text{ cm}$) sizes also can fit into the P-POD.

3.2. CalSat Description

CalSat is based on a 3U CubeSat, and all of the required CubeSat hardware is commercially available. The primary CalSat characteristics are summarized in Table 2.

³CubeSat requirements document: <http://www.cubesat.org/index.php/documents/developers>

Characteristic	Value
source frequencies [GHz]	47.1, 80.0, 140, 249 and 309
source spectral width [MHz]	< 1
output millimeter-wave power [mW]	50, 40, 3.2, 1.2 and 0.45
polarization	linear
cross-polarization level [dB]	-60
horn type	conical
input waveguide on horn	rectangular, single-moded
horn gain [dBi]	approximately 20
ADACS steering uncertainty [deg]	~1
ADACS attitude measurement uncertainty [deg]	0.05
polarization orientation uncertainty [deg]	0.05
estimated payload mass [kg]	0.8
estimated total CubeSat mass [kg]	3.8
calculated operating temperature [°C]	10 (night) to 30 (day)
orbit altitude [km]	500
orbital period [hours]	1.6
orbits per day	14.2

Table 2. CalSat characteristics. See Sections 3.2 & 3.4 for more detail.

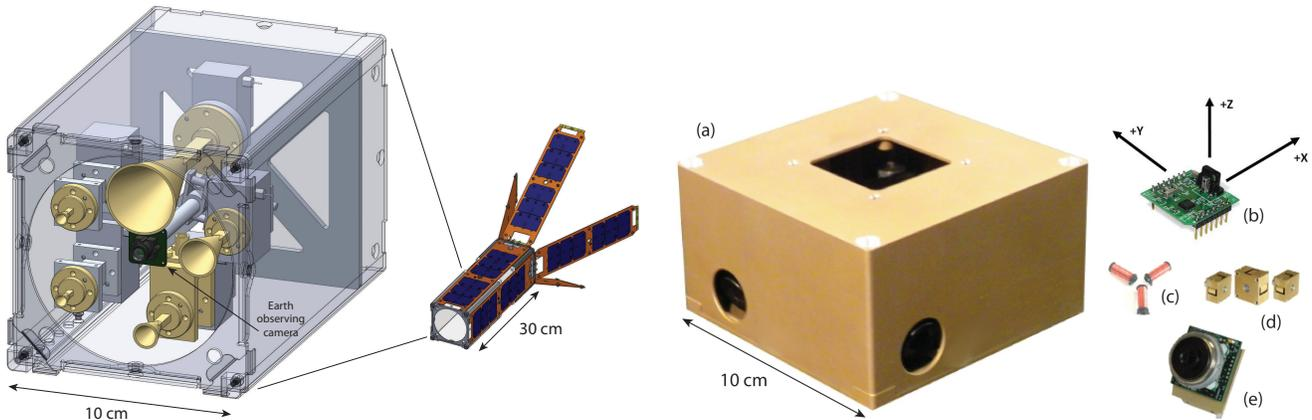


Fig. 3. **Left:** CalSat payload. The five horn antennas can be seen inside the circular aperture. From largest to smallest, the horns correspond to 47.1, 80.0, 140, 249 and 309 GHz. The associated Gunn oscillators and multipliers that produce the aforementioned five frequencies can be seen at the back of the horns. A thermal bus connects these sources together and to the payload walls. A polarizer mounted at the payload aperture ensures polarization purity. A control circuit powers and amplitude modulates the millimeter-wave sources each at a slightly different frequency. The thermal bus, polarizer and control circuit were removed from this figure to show millimeter-wave sources and to show clearly that they fit inside the small available volume. A schematic of the payload is shown in Figure 4. **Right:** The attitude determination and control system (ADACS). CalSat uses the MAI-400SS ADACS from Maryland Aerospace Inc., which is a turnkey system for CubeSats. The CubeSat attitude is measured with a magnetometer (b), star cameras (e) and Sun sensors, which are mounted near the solar panels. The CubeSat attitude is controlled with three reaction wheels (d) and magnetorquer rods (c), which move the CubeSat by torquing against the Earth’s magnetic field.

3.2.1. Bus/ADACS

The CalSat design uses the MISC3 3U CubeSat bus from Pumpkin Inc., which is a turnkey CubeSat kit that includes all of the aforementioned bus components. Pumpkin Incorporated was selected as the bus supplier for CalSat because their bus meets the pointing performance specification and more than ten of their CubeSats already have been successfully launched, therefore their hardware is well tested and comparatively low risk. The ADACS, which is manufactured by Maryland Aerospace Incorporated (MAI), is supplied by Pumpkin Inc. as part of their CubeSat kit. CalSat would use the MAI-400SS, which is a turnkey half-U (10 cm × 10 cm × 5 cm) subsystem that includes three reaction wheels, a three-axis magnetometer, two star cameras, three magnetorquer rods, sun sensors and an internal ADACS

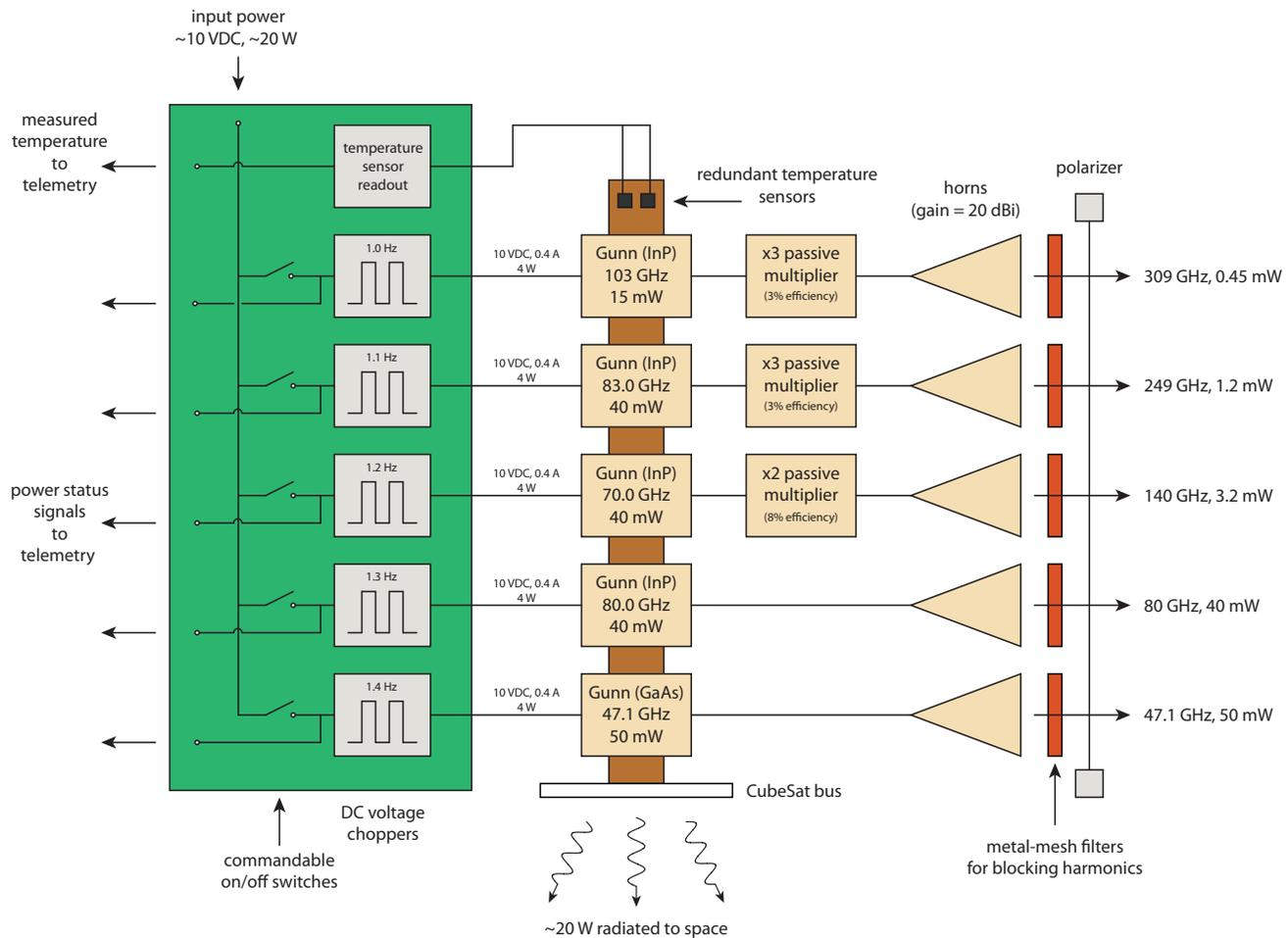


Fig. 4. A schematic of the CalSat payload. All five millimeter-wave tones are produced with Gunn oscillators. The three highest-frequency tones are produced with a passive doubler or tripler. The millimeter-wave power produced by each chain is given in the figure label. All five tones together require only 20 W of input DC power.

computer (see Figure 3). The magnetorquer rods are used to desaturate the reaction wheels by torquing the CubeSat against the magnetic field of the Earth. To operate this system, the user inputs the desired CalSat quaternion via the on-board computer, and the ADACS moves CalSat accordingly. The ADACS also continuously measures and outputs the attitude of CalSat. The selected MAI-400SS was designed to track latitude/longitude positions, so the firmware in this system already includes the operation mode that CalSat requires.

3.2.2. Payload

The calibration source in the payload consists of five amplitude modulated millimeter-wave “tones,” with one each at 47.1, 80.0, 140, 249 and 309 GHz. These five tones are designed to be well matched to (i) the observation windows in the atmospheric transmittance spectra, (ii) the Amateur Satellite Service bands in the Table of Frequency Allocations used by the Federal Communications Commission (FCC)⁴ and The National Telecommunications and Information Administration (NTIA)⁵, and (iii) the spectral bands commonly used in CMB polarimeters (more discussion in Section 5). A close-up view of the payload is shown in Figure 3. The 47.1 and 80.0 GHz tones are produced by Gunn diodes directly, while the 140, 249

⁴<http://www.fcc.gov>

⁵The United States Frequency Allocation Chart: <http://www.ntia.doc.gov/files/ntia/publications/2003-allochrt.pdf>

and 309 GHz tones are produced by pairing a Gunn diode with a passive multiplier. The 140 GHz tone is created by a 70 GHz Gunn diode and a passive doubler, the 249 GHz tone is created by an 83 GHz Gunn diode and a passive tripler, and the 309 GHz tone is created by a 103 GHz Gunn diode and a passive tripler. Suitable Gunn diodes and multipliers are readily available from Space Labs and Virginia Diodes Inc. (VDI), respectively. The tones above 47.1 GHz are produced by InP Gunn diodes because they output more millimeter-wave power. This additional power is useful because the required multipliers have conversion efficiencies of only 3 to 8 %. The additional power is not needed at 47.1 GHz, so a lower-power-output GaAs Gunn diode is used for this tone. Each tone would have an associated conical horn antenna that would emit a coherent, linearly polarized beam because the input waveguide of the horn is rectangular and single-moded. A small amount of the unwanted cross-polarization, approximately -30 dB, is produced by the horns adding uncertainty to the orientation of the calibration source off axis. Therefore, a wire-grid polarizer⁶ is installed at the payload aperture to suppresses this unwanted cross-polarization by an additional -30 dB or more for all five of the millimeter-wave sources. The final cross-polarization level is less than -60 dB, so 99.9999% of the power in the CalSat tones is emitted in a single polarization. The polarizer is installed with its transmission axis parallel to the co-polarization axis of the horn and slightly tilted to prevent standing waves between the horn and the polarizer. The millimeter-wave sources produce harmonics, so metal-mesh low-pass filters from QMC Instruments are mounted at the horn aperture of each source to eliminate any unwanted out-of-band radiation. It is important to emphasize that the CalSat tones are produced by commercially available components that are based on space-proven technologies, so the chance of a failure is comparatively low. Additional technical details are given in Table 2 and Figure 4. Alternative millimeter-wave sources such as broad waveguide-bandwidth noise sources were initially considered, but they are not compatible with the Table of Frequency Allocations used by the FCC and NTIA.

3.2.3. Ground Station

An S-band or UHF transmitter/receiver is used to communicate between the ground station and CalSat. Ground station hardware is commercially available from vendors like CubeSatShop⁷ or Clyde Space⁸. This radio link is used for downloading data and uploading commands. The higher frequency S-band link provides a faster data rate and it is only used if more data bandwidth is necessary. Amateur UHF or S-band radio frequencies are available for CubeSats. The CalSat ground station includes a web server. Spacecraft attitude data and other data products and software libraries are distributed to the scientific community from this server.

3.3. Pre-launch Testing

Prior to payload assembly, the horn beams are fully characterized, the source frequencies measured and the source beams mechanically aligned with the ADACS in the CalSat bus in the laboratory. The horn beams are mapped in two dimensions (θ, ϕ) with the antenna pattern measurement system shown in Figure 5. For this measurement, the CalSat millimeter-wave sources transmit power and are then pivoted about the phase center of the horn using a gimbal mount. A stationary receiver detects the emitted source power at each orientation. The gimbal mount is composed of two stepper-motor controlled rotation stages from Thor Labs. Both the co-pol and cross-pol beams are measured with this apparatus. The receiver in this system consists of a horn from Custom Microwave, a zero-bias Schottky diode detector from VDI and an isolator from Microwave Resources. The isolator inserted between the horn and the detector suppresses standing waves in the system. The beam mapping apparatus would need to be enclosed in a box lined with Eccosorb, which is a material that efficiently absorbs millimeter-waves [Peterson & Richards, 1984; Halpern *et al.*, 1986]. This baffle would ensure that reflected power does not produce spurious features in the beam map.

⁶<http://cosmology.ucsd.edu>

⁷<http://www.cubesatshop.com/>

⁸<http://www.clyde-space.com/>

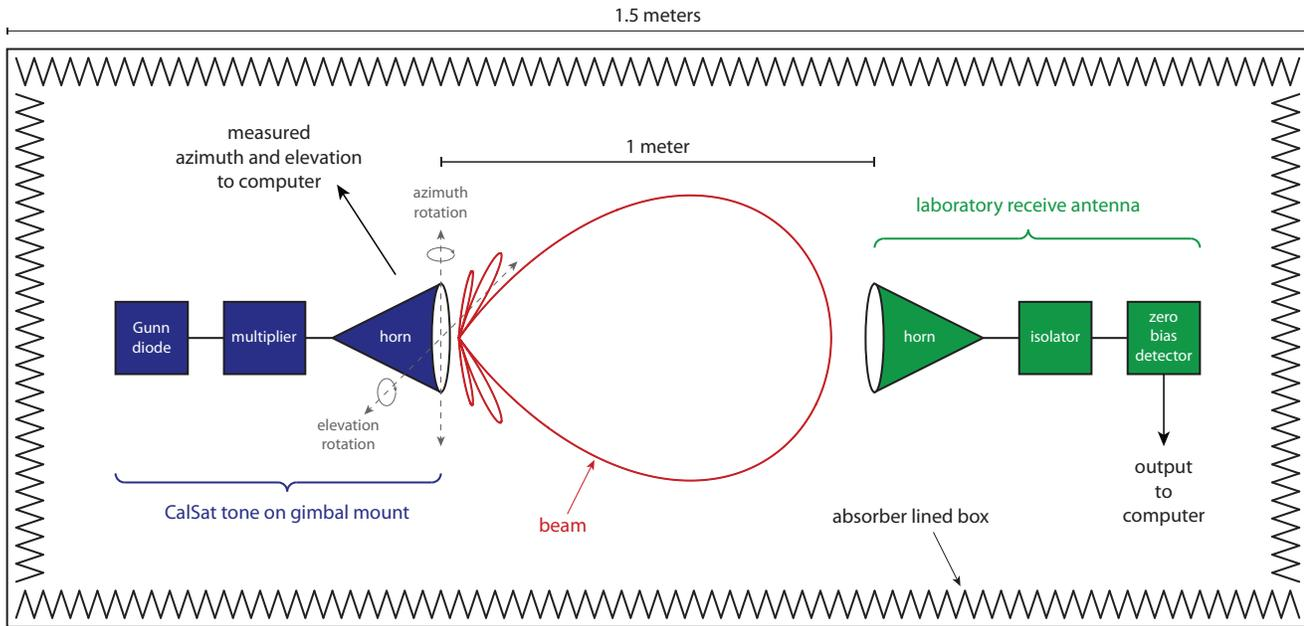


Fig. 5. Pre-launch beam map characterization measurement.

The millimeter-wave source frequencies are measured with a Fourier transform spectrometer (FTS). The receivers used in the beam mapping system are reused in this FTS measurement. This waveguide-bandwidth FTS measurement yields the precise frequency of each of the five tones with a very high signal-to-noise ratio. A second measurement is also done using the CalSat sources and a broadband 4 K bolometric receiver that can detect radiation below 650 GHz. For this second measurement, the source power is attenuated somewhat to match the dynamic range of the detector. This second measurement reveals any unwanted harmonics in the five tones, and it also shows that these harmonics are eliminated when the QMC Instruments filters are added.

The ADACS in the CalSat bus is designed to measure its own orientation to 0.05 deg. To ensure that the uncertainty in the polarization orientation of the CalSat tones is dominated by this ADACS pointing error the transmission axis of the polarizer in the payload must either be aligned to the ADACS reference system to better than 0.05 deg or the systematic offset angle between the two elements must be measured to better than 0.05 deg. Calculations show that aligning the polarizer to better than 0.05 deg would require micron precision, which should be achievable using standard precision metrology tools.

After CalSat is assembled, and the payload has been shown to work, the following required tests must be completed before launch: random vibration, sinusoidal vibration, shock, thermal vacuum cycle, thermal vacuum bake out, and a hardware configuration test. These tests are part of the CubeSat Program requirements and are defined by NASA's Launch Services Program (LSP). A specialized spacecraft testing facility, such as the facility at Cal Poly, is required for these tests.

3.4. *Launch, Orbit and Operations*

CalSat ideally will be placed in a polar orbit. A polar orbit is a particular type of low-Earth orbit (LEO) where a spacecraft travels in a north-south direction passing over both the north and south poles. Polar orbits are commonly used by Earth-observing satellites. While a spacecraft orbits in the north-south direction, the Earth moves beneath it in a west-east direction. If the precession rate of the orbit is phased appropriately, a satellite in a polar orbit will, over time, pass over the entire surface of the Earth. A conceptual diagram of this kind of orbit is shown in Figure 6. A polar orbit for CalSat ensures visibility from observatories in both the Northern Hemisphere, such as Mauna Kea in Hawaii and Summit Station in Greenland [Asada *et al.*, 2014], and the Southern Hemisphere, such as the Atacama Desert in Chile, and the

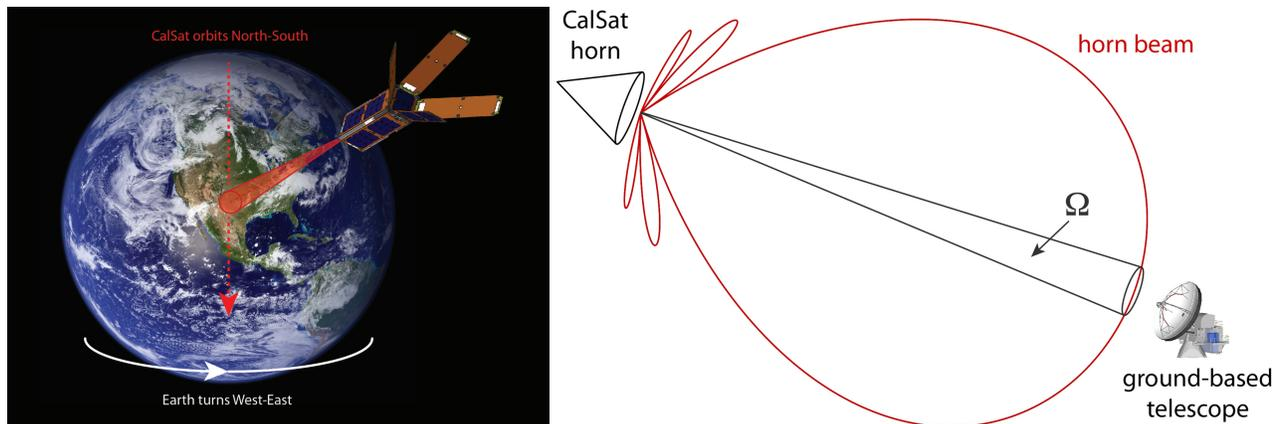


Fig. 6. **Left:** Schematic of CalSat operation. For clarity, only one of the five beams is shown. The calibration beam is pointed at the Earth, while the spacecraft is in a low-Earth, polar orbit traveling north-south. The Earth moves west-east below CalSat. If the precession rate of the orbit is phased appropriately, a satellite in a polar orbit like this one will, over time, pass over the entire surface of the Earth (see Figure 7). **Right:** A cross-sectional schematic diagram showing the coupling between one CalSat horn beam and a ground-based telescope. Only the emitted power inside the solid angle Ω is detected. See Section 4 and Equation 3 for more detail regarding the forecasted CalSat brightness from the power inside this solid angle.

South Pole. CalSat also will be observable by balloon-borne instruments flying from a range of locations, such as Ft. Sumner, New Mexico, Alice Springs, Australia and McMurdo Station in Antarctica. This global visibility makes CalSat the only source that can be observed by all terrestrial and sub-orbital millimeter-wave observatories. It is important to emphasize that a LEO does not have fixed Ra/dec coordinates on the sky, so CalSat would not permanently prevent a portion of the sky from being observed.

CalSat would be launched as an auxiliary payload on a DOD, NASA, or commercial rocket via launch programs such as NASA’s Educational Launch of Nanosatellites (ELaNa)⁹, NASA’s CubeSat Launch Initiative (CSLI)¹⁰ or the Air Force’s University Nanosat Program (UNP)¹¹. Because CalSat is launched as a flight of opportunity, the precise characteristics of the polar orbit, such as the altitude, can not be specified precisely before the launch opportunity is determined. Nevertheless, a target orbit is needed so the mission can be designed. We selected 500 km as the target altitude for the following three reasons. First, a 500 km orbit is achievable and viable. At approximately 1000 km the radiation environment substantially changes. Above 1000 km the Van Allen belts create a radiation environment that is too hostile for CubeSats. Below 1000 km the trace amount of atmosphere removes charged particles making the radiation density suitably low [Larson & Wertz, 1999]. Several existing CubeSats are in orbits with altitudes between 500 and 800 km. For comparison, the Hubble Space Telescope orbits at an altitude of 569 km. Second, at this altitude, air-drag becomes appreciable, and ultimately it can be used to de-orbit the CubeSat. Using the Drag Temperature Model (DTM) [King-Hele, 1987] we compute that the maximum expected lifetime of the CalSat orbit is approximately 16 years. This lifetime is compatible with the desired CalSat program, and it complies with the space debris guidelines established by the Inter-Agency Space Debris Coordination Committee (IADC) and the Office for Outer Space Affairs, which states that any CubeSat must de-orbit within 25 years of the end of its mission. Finally, performance forecasting studies show a 500 km altitude works well in terms of CalSat detectability (see Section 4). An altitude of 500 km corresponds to an orbital period of 1.6 hours, which means CalSat passes across the sky at the South Pole 14.2 times per day, and passes by other observatories several times per week (see Figure 7). The angular speed of CalSat varies with time as it passes by a given observatory. In Figure 8 we show the angular speed of CalSat as it passes by observatories at the South Pole and in the Atacama Desert in Chile. A typical CMB telescope should be able to track a source moving at these angular speeds.

⁹<http://www.nasa.gov/offices/education/centers/kennedy/technology/elana.feature.html>

¹⁰http://www.nasa.gov/directorates/heo/home/CubeSats_initiative.html

¹¹<http://prs.afrl.kirtland.af.mil/UNP/>

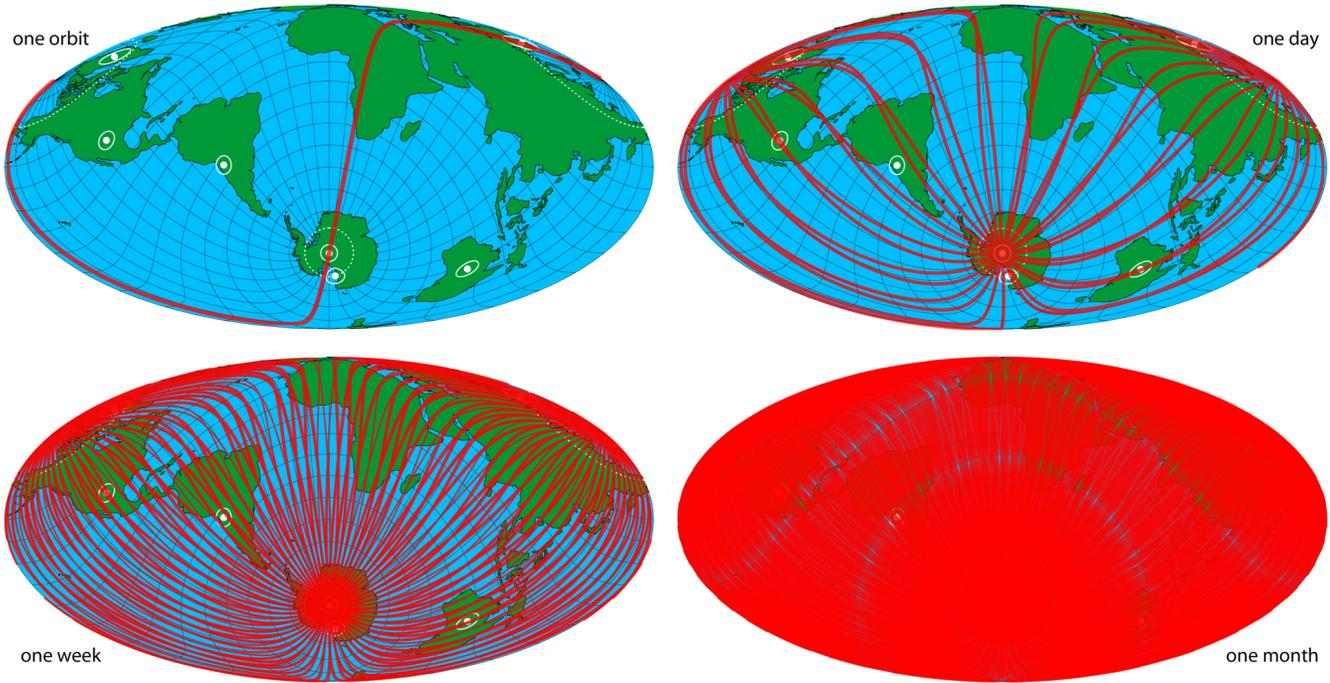


Fig. 7. CalSat orbits for 1.6 hours, one day, one week and one month. Observatories are marked with a white dot. The radius of the circle surrounding each observatory is 500 km, so when the red orbit curve is inside the white circle, then the local zenith angle of CalSat is 45 deg or less at that observatory because the altitude is also 500 km. The white dotted lines mark the approximate circumpolar trajectories of balloons launched from McMurdo Station in Antarctica and Kiruna, Sweden.

The location of CalSat is tracked by the North American Aerospace Defense Command (NORAD) and quantified by a six element state vector that includes position and velocity information. NORAD would provide the state vector, which is uploaded to CalSat by the ground station. The ADACS would then use this state vector in conjunction with sensor information to determine the attitude of the spacecraft. The on-board computer would also take this position information, determine which observatory is closest, and then point the calibration beams at that observatory. During operation, the CalSat beams are pointed at CMB observatories using the ADACS and then modulated at approximately 1 Hz. By modulating the amplitude of the tones, it is easier to detect them if the beam-filling atmospheric emission is fluctuating. The calibration beam attitude is updated in real time as CalSat moves past the observatory to ensure the millimeter-wave source beams are fixed on that observatory. It is important to point out that the polarization orientation of the millimeter-wave sources is not fixed in Ra/dec, and it will slowly drift relative to the reference frame of the observer as CalSat moves across the sky. However, this polarization orientation drift is always measured to 0.05 deg using the on-board star cameras, so this effect can be precisely accounted for during data analysis in the same way orientation drift is treated with celestial sources.

The measured attitude is recorded as a function of time and this time-ordered data is telemetered to the ground station each orbit. The downloaded data would immediately be made publicly available via a web server. The measured source beam patterns (see Section 3.3) and CalSat attitude data would then be used by the CMB community in the analysis of their calibration measurements. End users of our data would need the azimuth, elevation, polarization orientation and the anticipated source brightness of CalSat as a function of time. To facilitate use of our data, the CalSat team would write a software library that would compute these needed quantities for any given latitude and longitude, and this software library is distributed along with the data.

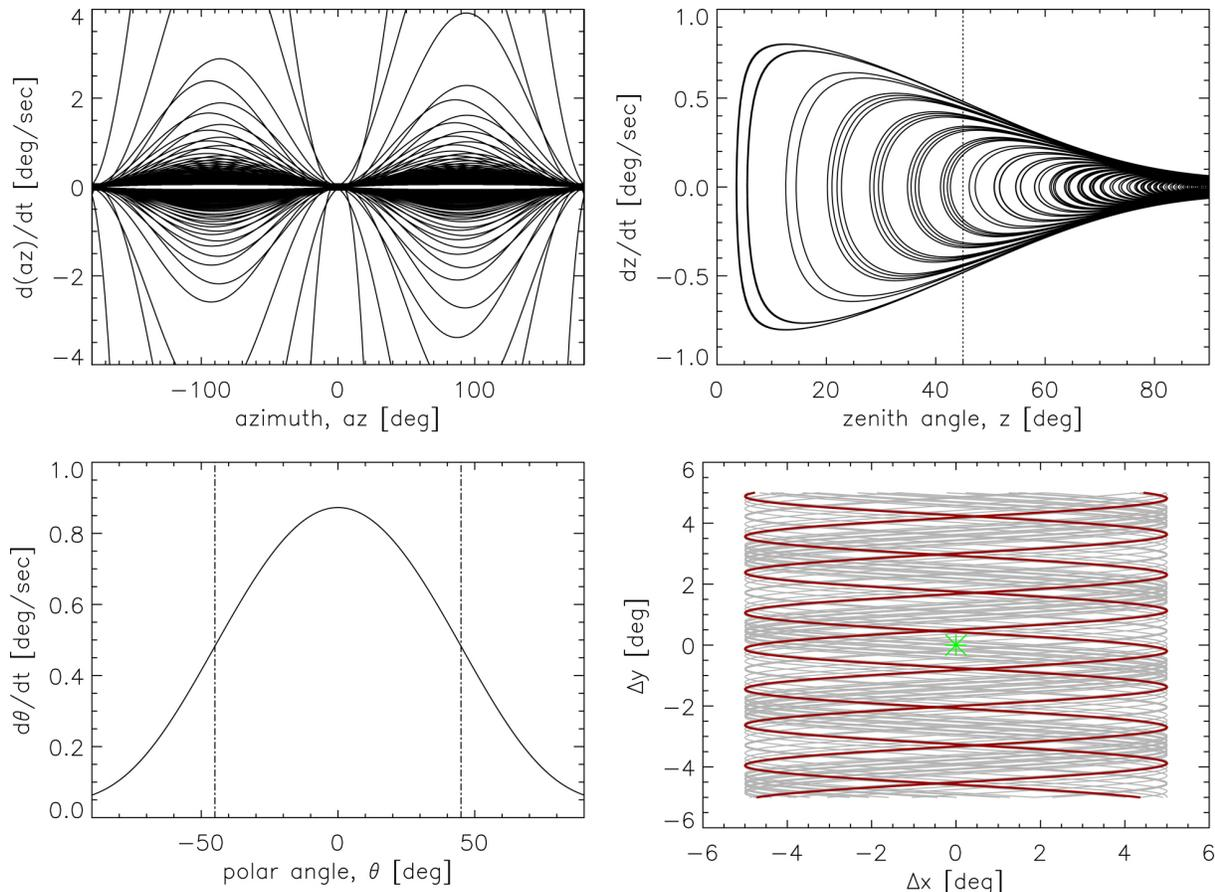


Fig. 8. **Top:** Angular speed of CalSat as observed from the Atacama Desert in Chile over one week. The motion is broken up into local azimuth (left) and zenith angle (right). **Bottom Left:** Angular speed of CalSat as observed from the South Pole. The azimuth angle is constant for each orbit, so the only motion to consider is the polar angle θ , which is positive when CalSat is approaching, zero during transit, and negative when leaving. **Bottom Right:** Boresite pointing for one day of CalSat observations from the South Pole. Here the telescope tracks CalSat in elevation from 30 to 70 deg, while scanning sinusoidally in azimuth. To achieve this pattern in the CalSat-centered frame, both the width of the azimuth throw of the telescope and the azimuth scan speed increase as the elevation angle increases, and the elevation angle speed of the telescope is slightly slower than that of CalSat, so CalSat passed through the field of view of the instrument. The red curve shows the scan pattern for a single orbit.

	peak power [W]	duty cycle [%]	average power [W]
payload	20	20	4.0
ADACS (MAI-400SS)	2.2	100	2.2
transceiver (Tx)	5.5	10	0.55
transceiver (Rx)	0.25	100	0.25
on-board computer	2.0	100	2.0
total	30		9.0

Table 3. CalSat power budget. The orbit average power was computed to be 12 W, and this should be compared with the 9 W of total average power in this table. CalSat should have 3.0 W of margin.

3.5. Power Budget

A breakdown of the power budget for CalSat is given in Table 3. For the mission to be sustainable, the orbit average power (OAP) must be greater than the average power consumption. In this limit, the solar panels are able to, on average, both power the CubeSat and keep the on-board battery charged. Here we computed the OAP as the sun/eclipse ratio times the average available power from the solar panels during sunlight time, assuming the Earth's albedo contribution is negligible during eclipse time. At 500 km, the sun/eclipse

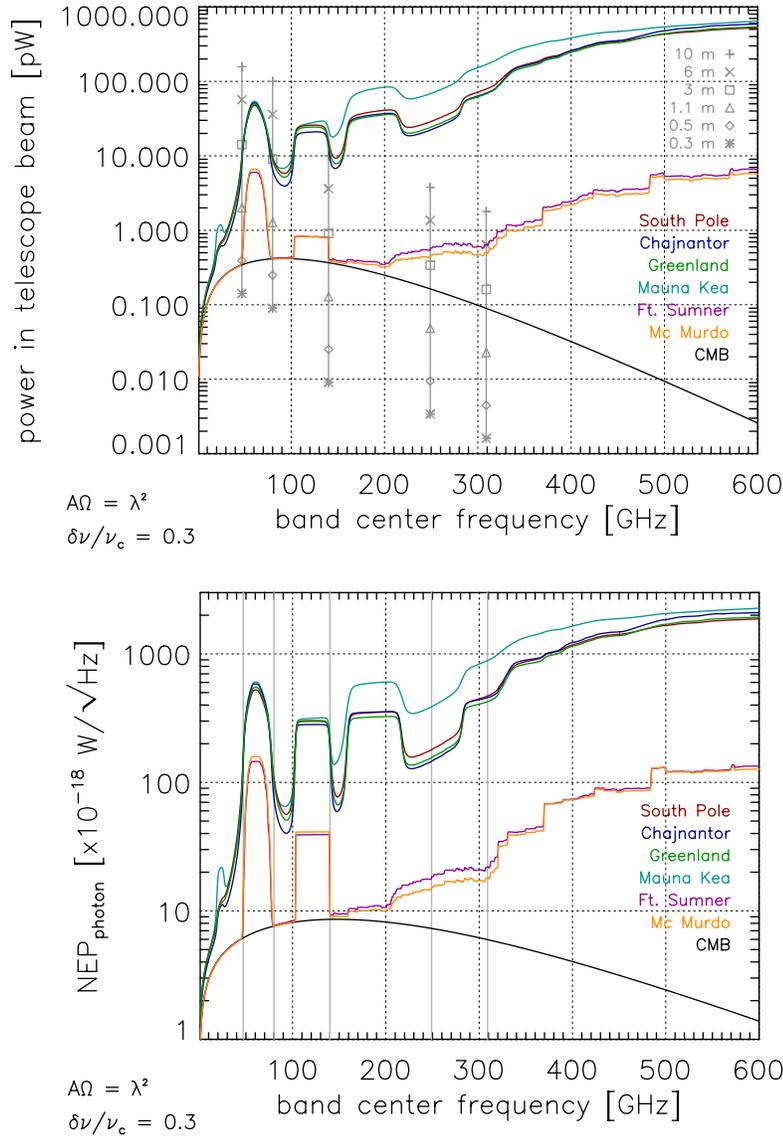


Fig. 9. CalSat detectability. These figures together show (i) that CalSat is detectable with high signal-to-noise, and (ii) that the power loading from CalSat can be compared with the power loading from the background, which is ideal. In the top panel we show the amount of millimeter-wave power CalSat would deliver to the telescope aperture. Six different telescope aperture diameters are indicated with symbols. The curves in this panel show the forecasted level of background power as a function of spectral band center frequency assuming some typical instrument characteristics and observatory conditions that are given in Section 4. For this analysis the background power comes from the CMB and the atmosphere. The bottom panel shows the expected photon NEP as a function of spectral band center frequency. As an example, a 150 GHz polarimeter with a 2.0 m aperture sited at the Llano de Chajnantor Observatory in the Atacama Desert would receive 10 pW of power from the sky, nearly 1 pW of power from CalSat, and the noise rms is $\sim 10^{-5}$ pW (assuming one second of integration with $\text{NEP}_{\text{photon}} = 10 \times 10^{-18} \text{ W}/\sqrt{\text{Hz}}$). Therefore the CalSat signal-to-noise ratio is 10^5 (or 50 dB) for this configuration. More signal-to-noise values computed from the information in these plots are given in Table 4.

ratio is 0.62. Given the number of solar panels in the MISC3 CubeSat, the solar panel configuration (see Figure 2), and assuming each 3U panel can provide 2 W of power, we computed that between 13 and 24 W is available depending on the orbit angle. The average available power is 20 W during sunlight time, which means the OAP is 12 W. Table 3 shows that the average power consumption is conservatively 9 W, so the CalSat mission is sustainable with approximately 3 W of margin.

Frequency [GHz]	Aperture [m]	South Pole	Chajnantor	Greenland	Mauna Kea	Ft. Sumner	McMurdo
47.1	0.3	31	31	31	31	42	41
47.1	0.5	35	36	35	35	47	46
47.1	1.1	42	43	43	42	54	53
47.1	3	51	51	51	51		
47.1	6	57	58	57	57		
47.1	10	61	62	61	61		
80.0	0.3	31	32	31	31	42	42
80.0	0.5	35	37	35	35	47	47
80.0	1.1	42	44	43	43	54	54
80.0	3	51	52	51	51		
80.0	6	57	58	57	57		
80.0	10	61	63	61	61		
140	0.3	18	18	18	17	30	30
140	0.5	22	23	22	22	34	34
140	1.1	29	30	30	29	41	41
140	3	38	38	38	37		
140	6	44	44	44	43		
140	10	48	49	49	48		
249	0.3	14	15	15	11	24	25
249	0.5	19	20	19	15	29	29
249	1.1	26	27	26	22	36	37
249	3	34	35	35	31		
249	6	40	41	41	37		
249	10	45	46	45	41		
309	0.3	7	7	7	4	20	21
309	0.5	11	11	12	9	25	25
309	1.1	18	18	19	16	32	32
309	3	27	27	27	24		
309	6	33	33	33	30		
309	10	37	37	38	35		

Table 4. Forecasted CalSat signal-to-noise ratio **in dB** for various observatories and telescope apertures. We assume the telescope zenith angle is 45 deg, and the CalSat altitude is 500 km. Here the signal-to-noise ratio is the peak signal divided by standard error of the mean for one second of integration. These ratios improve as the integration time increases and the telescope zenith angle approaches 0 deg.

4. Detectability

For CalSat to be useful, the detected calibration signal needs to be large when compared with the noise level of the calibration measurement. It is difficult to forecast the precise characteristics of every instrument that might observe CalSat. Therefore, to assess the detectability, three primary assumptions were made. First, we assumed the aperture diameter of any instrument observing CalSat is between 0.3 and 10 m, which is the current range for CMB experiments. Second, we assumed $A\Omega = \lambda^2$ and $\delta\nu/\nu_c = 0.3$. Here, A is the aperture area, Ω is the solid angle of the CMB telescope beam, and ν is the frequency of the incoming radiation with ν_c being the center frequency of the spectral band of the polarimeter. Third, we assumed the noise in the calibration measurement is dominated by photon noise from the CMB for balloon-borne measurements and the atmosphere for ground-based measurements.

To estimate the photon noise, spectral radiance curves were computed using the publicly available *am* atmospheric modeling software package¹². We used *am* version 8.0, which implements O₂ line mixing and non-resonant absorption near 60 GHz. Earlier versions of *am* did not model these effects, so these earlier versions had accuracy issues, which do not affect our calculations. The atmospheric profiles for the following six observatories were used in these simulations: South Pole, Chajnantor, Summit Station in Greenland, Mauna Kea, and balloon-borne observatories near Ft. Sumner, New Mexico, and McMurdo in Antarctica. For all sites, the zenith angle for observations was set to 45 deg. The altitude of the balloon-

¹²The *am* software: <https://www.cfa.harvard.edu/~spaine/am/>

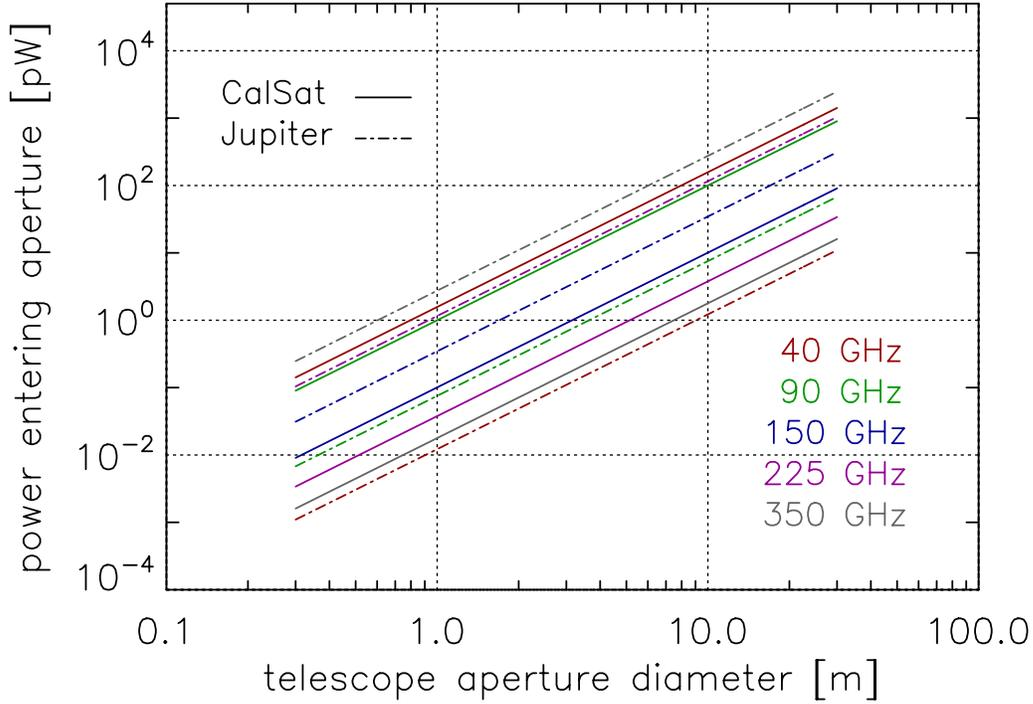


Fig. 10. Comparison between the power delivered by CalSat and the total power, integrated across the spectral band, from Jupiter. This comparison was computed for a range of telescope aperture diameters. When computing the curves for Jupiter we assumed $A\Omega = \lambda^2$, $\delta\nu/\nu_c = 0.3$ and the brightness temperature is 155 K for the 40 GHz spectral band and 173 K for the other spectral bands [Weiland *et al.*, 2011; Griffin *et al.*, 1986]. The CalSat curves are discussed in Section 4. An additional comparison between CalSat and Tau A is given in Table 1.

borne observatories was assumed to be 30 km. For the South Pole, Chajnantor, Greenland, and Mauna Kea observatories, the ambient temperature and PWV was assumed to be 230, 275, 248 and 275 K, and 1, 1, 1 and 4 mm, respectively. Given these conservative assumptions, the background power in the telescope beam and the associated photon noise equivalent power (NEP) were computed. The background power in the telescope beam was computed using

$$P_{\text{photon}} = \int Q(\nu) d\nu \text{ [W]}, \text{ where } Q(\nu) = \alpha \mathcal{T}(\nu) A\Omega \mathcal{B}(\nu). \quad (1)$$

and the photon NEP was computed using

$$NEP_{\text{photon}}^2 = 2 \int h\nu Q(\nu) d\nu + 2 \int \frac{c^2 Q(\nu)^2}{m A\Omega \nu^2} d\nu \text{ [W}^2/\text{Hz]}. \quad (2)$$

These equations are commonly used and their derivation can be found in the literature [Lamarre, 1986; Richards, 1994]. For our calculations, $\mathcal{B}(\nu)$ is the spectral radiance computed by *am*, $\mathcal{T}(\nu)$ is the spectral band-pass filter, which is a top-hat with a width equal to $\delta\nu/\nu_c = 0.3$ and $A\Omega = \lambda^2$. We assumed observations are made with detectors that are sensitive to a single-polarization, so $\alpha = 0.5$ and $m = 1$. The results are shown in Figure 9 and Table 4. The expected millimeter-wave power from CalSat at the telescope aperture was computed using the following equation:

$$P_{\text{CalSat}} = \frac{P_{\text{Gunn}}}{4\pi} 10^{g/10} \Omega \text{ [W]}, \text{ where } \Omega = \pi \left(\tan^{-1} \left(\frac{D}{2d} \right) \right)^2. \quad (3)$$

Here, P_{Gunn} is the millimeter-wave power from the source, g is the horn gain in dBi, D is the aperture diameter of the telescope, and d is the distance between CalSat and the telescope; Ω is the solid angle subtended by the telescope aperture as viewed from CalSat, and it is schematically shown in Figure 6.

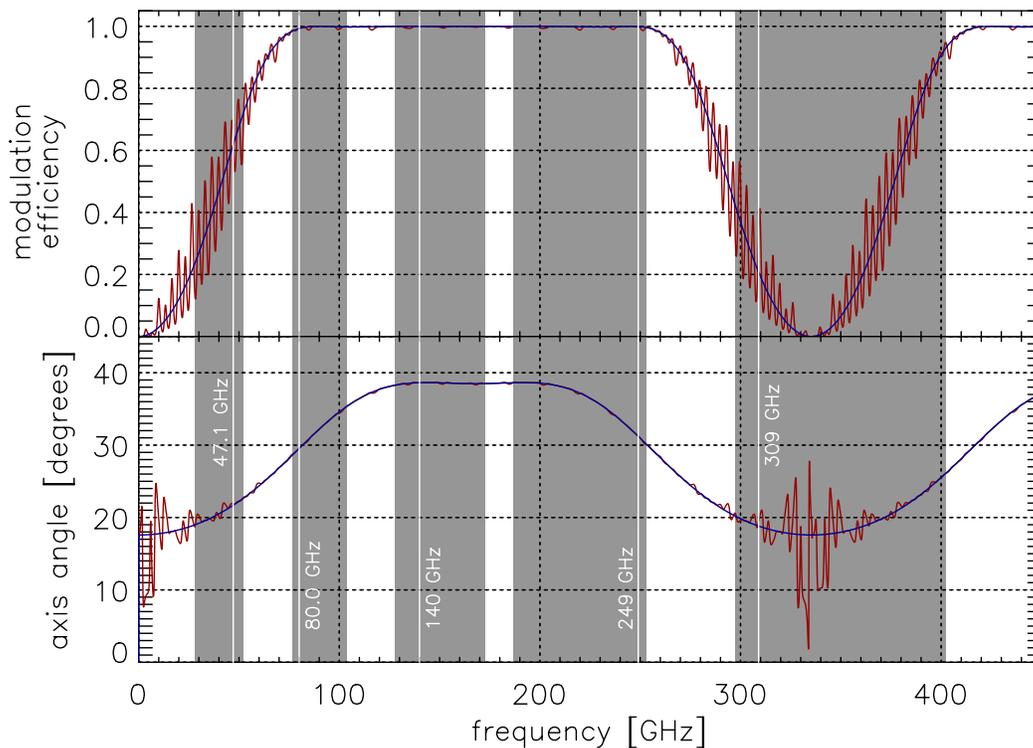


Fig. 11. One example showing the utility of CalSat. The plot shows simulated modulation efficiency and associated polarimeter axis curves for a five-crystal achromatic half-wave plate polarimeter [Savini *et al.*, 2006]. This kind of polarimeter has nearly perfect modulation efficiency across three spectral bands, which is attractive. However, the polarimeter axis varies with frequency by approximately 10 deg, and this axis angle needs to be calibrated to better than 0.2 deg. An observation of CalSat could constrain the axis-angle vs. frequency curve for this instrument. Note that if a celestial broadband source, such as Tau A, were used instead, the frequency spectrum of this celestial source would have to be precisely measured first to produce the same kind of constraint.

The power arriving in the telescope aperture from CalSat is plotted versus telescope aperture diameter in Figure 10. For comparison, the power arriving in the telescope aperture from Jupiter, which is a bright and commonly used *unpolarized* calibrator, was also computed and plotted alongside the CalSat curves in this Figure.

This analysis shows that (i) the brightness of CalSat is similar to the brightness of the background, (ii) the brightness of CalSat is comparable to Jupiter, and (iii) the signal-to-noise ratio for one second of integration is typically between 1,000 and 100,000. These are all characteristics of an ideal calibration source. If CalSat were significantly brighter than the background then the signal would likely saturate the detectors (assuming TES bolometers are being used, which is the current standard at these frequencies).

The CalSat instrument configuration presented in this paper was designed to support the following ongoing experiments and any associated follow-up experiments from these collaborations: ACT [Naess *et al.*, 2014], BICEP/KECK [Ahmed *et al.*, 2014; Buder *et al.*, 2014], CLASS [Essinger-Hileman *et al.*, 2014], GroundBIRD [Tajiman *et al.*, 2012], EBEX [Reichborn-Kjennerud *et al.*, 2010], PIPER [Lazear *et al.*, 2014], POLARBEAR [Arnold *et al.*, 2014; Tomaru *et al.*, 2012; Kermish *et al.*, 2012], QUIJOTE [Perez-de-Taoro *et al.*, 2014], SPIDER [Rahlin *et al.*, 2014], and SPTPol [Benson *et al.*, 2014; Austerman *et al.*, 2012]. Additional experiments that could use CalSat are being designed: GLP [Araujo *et al.*, 2014], SKIP [Johnson *et al.*, 2014], and QUBIC [Ghribi *et al.*, 2014]. And the planned CMB-S4 [Abazajian *et al.*, 2015b] program would benefit from CalSat because it could be used to both accurately calibrate deep observations and combine results from different observatories. Though CalSat is designed for CMB polarization experiments, it could also straightforwardly be used to calibrate other observatories such as ALMA and the VLA.

5. Discussion

As a narrow-band source, CalSat is not designed to characterize the broad-band spectral properties of CMB polarimeters. Instead it is designed to provide the critical relationship between the coordinate system of the polarimeter in the instrument frame and the coordinate system on the sky that defines the astrophysical Q and U Stokes parameters. The spectral bands in CMB polarimeters are typically broad, and some polarimeter technologies, such as the achromatic half-wave plate and the sinuous antenna multi-chroic pixel, have frequency dependent performance. Therefore polarimeter calibration must be performed over the full spectral bandwidth for experiments using these technologies. CMB experiment teams must characterize the spectral properties of their instruments in the laboratory before deployment and then use the clean and simple CalSat signals together with their lab-based instrument transfer functions during their calibration analyses. For example Figure 11 shows simulated modulation efficiency and polarimeter axis angle curves for an achromatic half-wave plate polarimeter. The 80.0, 140 and 249 GHz CalSat tones could be used to verify that the modulation efficiency is very close to unity at these frequencies and the polarimeter axis varies as expected as a function of frequency.

CalSat is programmed to listen for the ground station each orbit. If the radio uplink from the ground station fails, then the on-board computer turns the CalSat tones off and wait for the link to be restored. This mode of operation guards against out-of-control behavior. If this program malfunctions and the tones stay on, then the batteries will drain and the instrument will shutdown because the power budget can not support continuous operation. Therefore, the most likely failure mode is CalSat would turn off within 24 hours and then de-orbit 16 years later.

The selected tones match the Amateur Satellite Service Bands as stated in the text. We chose to use these bands because there is already an international agreement in place that allows instruments like CalSat to broadcast in these bands. It is possible to request permission to broadcast using other frequencies for a limited time by applying for an “experimental” license from the FCC¹³. We avoided using this approach as a baseline plan because there is some risk involved. Projects using experimental licenses cannot cause interference and they cannot request protection from interference. The aforementioned Table of Frequency Allocations shows that below 300 GHz, all frequencies are already allocated, so interference is possible. Nevertheless, if CalSat moves forward, every effort will be made to maximize the utility of the instrument by adjusting the frequencies so they accommodate all possible users.

All experiments trying to extract cosmological information from the TB, EB and B-mode signals need a robust polarimeter calibration program that will allow the effect of instrument-induced errors to be mitigated during data analysis. A robust mitigation strategy for IPR, which is one of the most critical systematic errors, has not yet been identified because a suitable celestial calibration source does not exist and ground-based solutions are challenging. Moreover, the commonly used self-calibration technique, that uses the TB and EB spectra to remove any spurious B-mode signals, prohibits B-mode measurements from constraining the aforementioned isotropic departures from the standard model. CalSat was designed to be a low-cost, open-access solution to the IPR calibration problem for the CMB community, and its global visibility makes CalSat the only source that can be observed by all terrestrial and sub-orbital experiments. This global visibility makes CalSat a powerful universal standard that permits comparison between experiments from different observatories using appreciably different measurement approaches.

6. Acknowledgements

Johnson, Keating and Kaufman acknowledge support from winning a Buchalter Cosmology Prize (Second Prize) in 2014 for their paper entitled “Precision Tests of Parity Violation Over Cosmological Distances” [Kaufman *et al.*, 2014]. This paper explores the idea of using TB and EB spectra to study new physics via CPR, and these kinds of measurements rely on precise calibration enhancements; CalSat was used as an example of an enhanced calibration technique in this paper. We would like to thank Ari Buchalter and the Buchalter Cosmology Prize Advisory Board and Judging Panel for acknowledging our work with this prize.

¹³FCC Public Notice DA:13-445

References

- Abazajian, K. N., et al. [2015a] *Astroparticle Physics* **63**, 6680.
- Abazajian, K. N., et al. [2015b] *Astroparticle Physics* **63**, 55-65.
- Adam, R., et al. [2014] *A&A*, submitted.
- Ahmed, Z., et al. [2014] *Proc. SPIE* **9153**, 91531N.
- Araujo, D., et al. [2014] *Proc. SPIE* **9153**, 91530W.
- Arnold, K., et al. [2014] *Proc. SPIE* **9153**, 91531F.
- Asada, K., et al. [2014] *Proc. SPIE* **8444**, 84441J.
- Aumont, J., et al. [2010] *A&A* **510**, A70.
- Austermann, J. E., et al. [2012] *Proc. SPIE* **8452**, 84521E.
- Baumann, D., et al. [2009] *AIP Conf. Proc.* **1141**, 10.
- Bennett, C. L., et al. [2013] *ApJS* **208**, 20B.
- Benson, B. A., et al. [2014] *Proc. SPIE* **9153**, 91531P.
- BICEP2 Collaboration [2014] *Phys. Rev. Lett.* **112**, 241101.
- BICEP2 Collaboration [2014] *ApJ* **792**, 62.
- BICEP2/Keck and Planck Collaborations [2015] *Phys. Rev. Lett.* **114**, 101301.
- Bock, J., et al. [2006] "Task Force on Cosmic Microwave Background Research." (arXiv:astro-ph/0604101).
- Bock, J., et al. [2009] "Study of the Experimental Probe of Inflationary Cosmology (EPIC)-Intermediate Mission for NASA's Einstein Inflation Probe." (astro-ph/0906.1188).
- Brown, M. L., et al. [2009] *ApJ* **705**, 978.
- Buder, I., et al. [2014] *Proc. SPIE* **9153**, 915312.
- Carroll et al. [1991] *Phys. Rev. D* **43**, 12.
- Crites et al. [2015] *ApJ* **805**, 36.
- Essinger-Hileman, T., et al. [2014] *Proc. SPIE* **9153**, 91531I.
- Ghribi, A., et al. [2014] *Journal of Low-Temperature Physics* **176**, 5-6, 698-704.
- Gluscevic, V. and Kamionkowski, M. [2010] *Phys. Rev. D* **81**, 12.
- Griffin, M. J., et al. [1986] *ICARUS* **65**, 244-256.
- Halpern, M., et al. [1986] *Applied Optics* **25**, 4.
- Johnson, B. R., et al. [2014] *Journal of Low-Temperature Physics* **176**, 5-6, 741-748.
- Keisler, R., et al. [2015] *ApJ* **807**, 151.
- Kamionkowski, M., Kosowsky, A. & Stebbins, A. [1997] *Phys. Rev. D* **55**, 7368.
- Kaufman, J., Keating, B. G. & Johnson, B., R., [2015] *MNRAS submitted* arXiv:1409.8242.
- Keating, B. G., Shimon, M., & Yadav, A. P. S., [2013] *ApJL* **762**, L23.
- Kermish, Z., et al. [2012] *Proc. SPIE* **8452**, 84521C.
- King-Hele, D. G. [1987] *Satellite Orbits in an Atmosphere: Theory and application*, (Springer).
- Knox, L. & Song, Y. [2002] *Phys. Rev. Lett.* **89**, 011303.
- Lazear, J., et al. [2014] *Proc. SPIE* **9153**, 91531L.
- Lamarre, J. M. [1986] *Applied Optics* **25**, 6.
- Larson, W. J. & Wertz, J. R. [1999] *Space Mission Analysis and Design (Third Edition)*, eds. Larson, W. J. & Wertz, J. R. (Microcosm).
- Naess et al. [2014] *J. Cosmol. Astropart. Phys.* **2014**, 10.
- Ni, W. [1977] *Phys. Rev. Lett.* **38**, 7.
- O'Dea, D., Challinor, A., & Johnson, B. R. [2007] *MNRAS* **376**, 1767.
- Perez-de-Taoro, M. R., et al. [2014] *Proc. SPIE* **9145**, 91454T.
- Peterson, J. B. & Richards, P. L. [1984] *Int. J. Infrared Millimeter Waves* **5**, 1507.
- Planck Collaboration [2014] *A&A* **571**, A1.
- Planck Collaboration [2015] *A&A submitted* arXiv:1507.02058v1.
- Pogosian, L., et al. [2009] *JCAP* **2**, 13.
- The POLARBEAR Collaboration [2014] *ApJ* **794**, 171.
- QUIET Collaboration [2011] *ApJ* **741**, 111.
- Rahlin, A. S., et al. [2014] *Proc. SPIE* **9153**, 915313.
- Reichborn-Kjennerud, B., et al. [2010] *Proc. SPIE* **7741**, 77411C.
- Richards, P. L. [1994] *J. Appl. Phys.* **76**, 1.
- Savini, G., Pisano, G., & Ade, P. A. R. [2006] *Applied Optics* **45**, 35.
- Smith, K. M., et al. [2012] *JCAP* **6**, 14.

- Tajiman, O., *et al.* [2012] *Proc. SPIE* **8452**, 84521M.
Tomaru, T., *et al.* [2012] *Proc. SPIE* **8452**, 84521H.
Weiland, J. L., *et al.* [2011] *ApJS* **192**, 19.
Yadav, A., *et al.* [2012] *Phys. Rev. D* **86**, 12.
Zaldarriaga, M. & Seljak, U. [1997] *Phys. Rev. D* **55**, 4.